Modern Physics Letters A,


# RESULTS FROM AMANDA*

CHRISTOPHER WIEBUSCH

*CERN EP-Div., 1211 Geneva 23, Switzerland*

for the AMANDA COLLABORATION

*J. Ahrens[11], X. Bai[1], S.W. Barwick[10], T. Becka[11], K.-H. Becker[2], D. Bertrand[3], E. Bernadini[4], F. Binon[3], A. Biron[4], S. Böser[4], O. Botner[16], A. Bouchta[4,†] O. Bouhali[3], T. Burgess[17], S. Carius[6], T. Castermans[12], A. Chen[14], D. Chirkin[9,2], J. Conrad[16], J. Cooley[14], D.F. Cowen[8], A. Davour[16], C. De Clercq[18], T. DeYoung[14,‡], P. Desiati[14], J.-P. Dewulf[3], P. Doksus[14], P. Ekström[17], T. Feser[11], T.K. Gaisser[1], M. Gaug[4,§] L. Gerhardt[10], A. Goldschmidt[7], A. Hallgren[16], F. Halzen[14], K. Hanson[14], R. Hardtke[14], T. Hauschildt[4], M. Hellwig[11], P. Herquet[12], G.C. Hill[14], P.O. Hulth[17], S. Hundertmark[17], J. Jacobsen[7], A. Karle[14], B. Koci[14], L. Köpke[11], M. Kowalski[4], K. Kuehn[10], J.I. Lamoureux[7], H. Leich[4], M. Leuthold[4], P. Lindahl[6], I. Liubarsky[5], J. Madsen[15], P. Marciniewski[16], H.S. Matis[7], C.P. McParland[7], Y. Minaeva[17], P. Miočinović[9], P.C. Mock[10,¶] R. Morse[14], R. Nahnhauer[4], T. Neunhöffer[11], P. Niessen[18], D.R. Nygren[7], H. Ogelman[14], Ph. Olbrechts[18], C. Pérez de los Heros[16], A.C. Pohl[6], P.B. Price[9], G.T. Przybylski[7], K. Rawlins[14], E. Resconi[4], W. Rhode[2], M. Ribordy[4], S. Richter[14], J. Rodríguez Martino[17], D. Ross[10], H.-G. Sander[11], T. Schmidt[4], D. Schneider[14], R. Schwarz[14], A. Silvestri[10], M. Solarz[9], G.M. Spiczak[15], C. Spiering[4], D. Steele[14], P. Steffen[4], R.G. Stokstad[7], P. Sudhoff[4], K.-H. Sulanke[4], I. Taboada[13], L. Thollander[17], S. Tilav[1], C. Walck[17], C. Weinheimer[11], C.H. Wiebusch[4,†], C. Wiedemann[17], R. Wischnewski[4], H. Wissing[4], K. Woschnagg[9], G. Yodh[10], S. Young[10]*

*(1) Bartol Research Institute, University of Delaware, Newark, DE 19716, USA*
*(2) Fachbereich 8 Physik, BUGH Wuppertal, D-42097 Wuppertal, Germany*
*(3) Université Libre de Bruxelles, Science Faculty CP230, B-1050 Brussels, Belgium*
*(4) DESY-Zeuthen, D-15735 Zeuthen, Germany*
*(6) Dept. of Technology, Kalmar University, S-39182 Kalmar, Sweden*
*(7) Lawrence Berkeley National Laboratory, Berkeley, CA 94720, USA*
*(8) Dept. of Physics, Pennsylvania State University, University Park, PA 16802, USA*
*(9) Dept. of Physics, University of California, Berkeley, CA 94720, USA*
*(10) Dept. of Physics and Astronomy, University of California, Irvine, CA 92697, USA*
*(11) Institute of Physics, University of Mainz, Staudinger Weg 7, D-55099 Mainz, Germany*
*(12) University of Mons-Hainaut, 7000 Mons, Belgium*
*(13) Departamento de Física, Universidad Simón Bolívar, Apdo. Postal 89000, Caracas, Venezuela*
*(14) Dept. of Physics, University of Wisconsin, Madison, WI 53706, USA*
*(15) Physics Dept., University of Wisconsin, River Falls, WI 54022, USA*
*(16) Division of High Energy Physics, Uppsala University, S-75121 Uppsala, Sweden*
*(17) Dept. of Physics, Stockholm University, SCFAB, SE-10691 Stockholm, Sweden*
*(18) Vrije Universiteit Brussel, Dienst ELEM, B-1050 Brussel, Belgium*

Received (received date)
Revised (revised date)

*Talk given at CERN EP seminar September 2001
†Present address: CERN, CH-1211, Geneva 23, Switzerland
‡Present address: Inst. for Part. Physics, University of California, Santa Cruz, CA 95064, USA
§Present address: IFAE, Campus UAB, 08193 Bellaterra, Spain
¶Present address: Science & Engin. Assoc. Inc., 7545 Metropolitan Dr., San Diego, CA 92108, USA

The **A**ntarctic **M**uon **a**nd **N**eutrino **D**etector **A**rray (AMANDA) is a high-energy neutrino telescope operating at the geographic South Pole. It is a lattice of photo-multiplier tubes buried deep in the polar ice. The primary goal of this detector is to discover astrophysical sources of high energy neutrinos. We describe the detector methods of operation and present results from the AMANDA-B10 prototype. We demonstrate the improved sensitivity of the current AMANDA-II detector. We conclude with an outlook to the envisioned sensitivity of the future IceCube detector.

*Keywords*: Astroparticle Physics, AMANDA, IceCube, Neutrino, South Pole, AGN
*PACS Nos.*: 95.55.Vj, 95.85.Ry and 96.40.Tw

## 1. Introduction

High-energy cosmic ray particles, nuclei, gammas and neutrinos, carry information about high energy phenomena in the universe in the TeV to the EeV energy range. While neutrinos are the most difficult to detect, they could provide the most natural information about their production sites, since they travel undisturbed to Earth. They are not affected by absorption within the source nor during propagation, and they are not deflected by magnetic fields. The distance at which the high energy universe can be observed with neutrinos is only limited by the signal strength of the source.

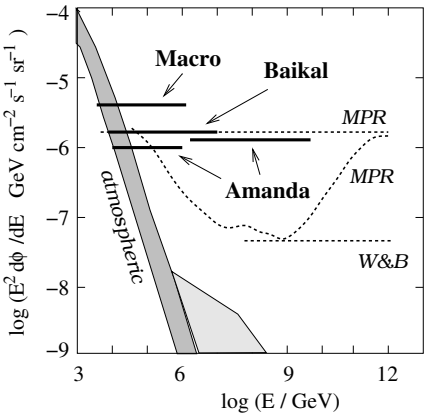


Fig. 1. Expectations and bounds on high-energy neutrino ($\nu_\mu + \bar{\nu}_\mu$) fluxes. Shown are the experimental limits from AMANDA (see section 4.2), BAIKAL[1] and Macro[2]. The grey bands denotes the flux of atmospheric neutrinos (with the excess at high energies from charm decays). W&B corresponds to an upper bound derived by normalizing the neutrino flux to the observed flux of cosmic rays.[3] Reasonable assumptions can loosen this bound, indicated by the two lines MPR.[4]

Many models of energetic astrophysical sources predict the emission of high-energy neutrinos (see figure 1).[5,6] Most of them assume acceleration of protons by shock waves. High-energy neutrinos are then produced in decays of mesons, which themselves are results of interactions of the high-energy protons with ambient matter or

dense photon fields. The neutrino energy spectrum follows the hard spectrum of the primary protons. Tau neutrinos are suppressed due to the larger production threshold of charmed mesons. Analysis of the decay chains predicts the ratios of produced neutrino flavors: $\nu_\mu : \nu_e : \nu_\tau \simeq 2 : 1 : 0$ at the source. However, neutrino oscillations would lead to full mixing of all flavors, because of the long distance from the source; and the ratios at the earth should be: $1 : 1 : 1$. Therefore experiments should be optimized to detect all three flavors.

Neutrinos are difficult to detect, and the predicted fluxes are low. Several potential detection techniques are described in Ref.[7]. A common method is to instrument a large volume of natural water or ice with a lattice of large area photo-multipliers tubes, which detect the Cherenkov light produced by the charged secondaries from a neutrino interaction in or close to the detector.

The two projects: BAIKAL[1], located in the deep natural lake Baikal, and AMANDA[8], located in the deep Antarctic ice at the geographical South Pole, have installed permanently operating detectors. Comparable experiments in the Mediterranean are in preparation[9]. The next step is the construction of a much larger experiment with a volume of about one cubic kilometer: IceCube[10] at the South Pole. This size seems adequate[5,6] to challenge existing neutrino flux predictions and to extend the sensitivity to all neutrino flavors.

The main emphasis of this paper is on the results obtained with the data from the AMANDA-B10 experiment in 1997, its first year of full operation. These results demonstrate that the operation of a huge neutrino detector with a sufficient understanding of the open environment is feasible. The extrapolation of these results to estimate the performance of the 2nd phase detector AMANDA-II are verified with the first data from that detector, obtained in the year 2000. Present assumptions on the performance of the IceCube experiment are based on this solid experimental ground.

## 2. Under-ice -water Neutrino Telescopes: Principles of Operation

### 2.1. *Signal signatures*

The main neutrino detection channel is a charged current interaction with a nucleon $N$ of the ambient detection medium

$$\nu_l + N \longrightarrow l + X \ , \tag{1}$$

in which a charged lepton $l$ and a hadronic cascade $X$ are produced. The direction of the lepton is aligned with the neutrino direction with a mean angle[5]

$$\langle \psi(\nu, l) \rangle \simeq \left( \frac{0.7^\circ}{E_\nu / \mathrm{TeV}} \right)^{0.7} \ . \tag{2}$$

Each neutrino flavor $l = e, \mu, \tau$, generates a different detection signature — they are sketched in figure 2.

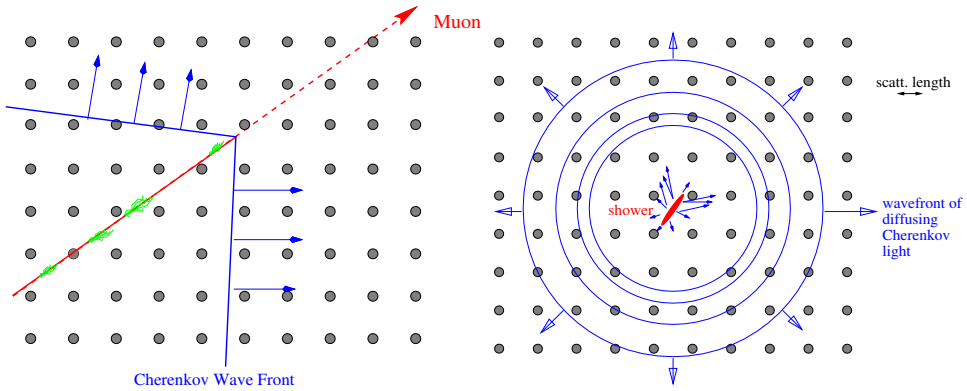


Fig. 2. Detection signatures for tracks (left) and cascades (right).

Traditionally favored is the $\nu_\mu$ channel, which leads to a high-energy $\mu$ track. The muon can propagate several kilometers through the ice before it reaches the instrumented volume of the detector. The effective experimental volume is thus much larger than the detector itself. The relativistic muon generates a cone of Cherenkov light, which is emitted at fixed angle $\theta_c$, given by the index of refraction $n_{ice}$ in the ice: $\cos\theta_c = 1/n_{ice} \approx 0.75$. The time and amplitude of detected signals are used to reconstruct the motion of the Cherenkov cone through the detector.

Secondary radiative energy loss processes lead to secondary charged tracks along the muon trajectory, which also produce Cherenkov light. This additional light can be used to measure the muon energy at the detector. However, the resolution is limited by fluctuations of these processes. Futhermore, this energy estimate is only a lower bound on the neutrino energy, because it only includes energy emitted inside the detector, and the interaction vertex is often far away.

The other two channels $\nu_e$ and $\nu_\tau$ are different. An electron, produced by a $\nu_e$, will generate an electro-magnetic cascade, which is confined to a volume of a few cubic meters. It overlays the hadronic cascade $X$ of the primary interaction vertex. The sizes of both cascades are small compared to the granularity of the PMT spacing. The signature is an expanding spherical shell of Cherenkov photons with a larger intensity in the forward direction. A tau, produced by a $\nu_\tau$, will decay immediately and generate a second hadronic cascade. However, at energies $> 1\,\mathrm{PeV}$ the two cascades are separated by several tens of meters, connected by a single track. This signature of two, extremely bright, hadronic cascades is unique for $\nu_\tau$ and is called a *double bang event*.

The measurement of these events is restricted to interactions close to the detector, thus requiring larger instrumented volumes than for $\nu_\mu$ detection. Also the accuracy of the direction measurement is worse for cascades than for long muons tracks. However, in case of diffuse fluxes the $\nu_e$ and $\nu_\tau$ channels also have clear advantages.

The backgrounds from atmospheric neutrinos are smaller. The energy resolution is significantly better, since the full energy is deposited in the detector. The cascade channel is sensitive to all neutrino flavors because of neutral current interactions.

### 2.2. *Backgrounds*

AMANDA searches for extremely rare signals. Consequently backgrounds are a major concern, which strongly depend on the specific subject of analysis. However, two major backgrounds are common to all analyses. They are shown in figure 3 and shall be discussed here:

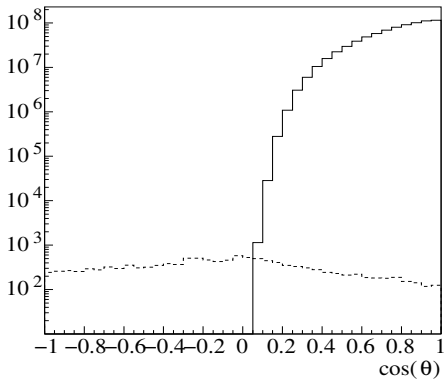


Fig. 3. Atmospheric muons (solid line) and atmospheric neutrino induced muons (dotted line) as function of the zenith angle. Shown is a MC simulation of the number of events, triggered in 130 days of AMANDA-B10 operation in 1997. $\cos\theta = 1$ corresponds to vertically down-going tracks.

(i) Down-going atmospheric muons.
High-energy muons generated in cosmic ray air showers can penetrate deep underground to depths larger than 10 km. They appear as single muon track or as bundle of aligned muon tracks. They are the most abundant triggered signal in AMANDA. Their rate falls strongly with the depth, the muon energy and zenith angle. At low energies an up-going muon is a clear signature for a neutrino interaction, since only neutrinos can penetrate the Earth. At large energies ($>$ PeV), the background from down going muons becomes smaller and the field of view can be extended to the upper hemisphere. However, the Earth also becomes opaque to neutrinos, which reduces the signal from the lower hemisphere.

(ii) Muons from atmospheric neutrinos
High-energy neutrinos are also generated in cosmic ray air showers. Muons induced by these neutrinos can arrive from the lower hemisphere. They form an unavoidable background to any search for celestial neutrinos. Fortunately, they have a softer energy spectrum than expected celestial neutrino sources,

and they can be suppressed by the selection of high energy events.
This neutrino background is the best known source of neutrino induced upward going muons. Their absolute flux is uncertain by $\simeq 30\%$ and the angular shape by about 5%.[12] They are an important calibration tool for the performance of the experiment and the sensitivity to neutrino induced muons.

### 2.3. *Signal search strategies*

The optimum analysis strategy depends on the desired signal and its backgrounds, and the detector performance, e.g. the effective volume, varies strongly with signal type. The signal types and backgrounds are summarized in Table 1.

Table 1. Signal search strategies. The possibility to use various potential analysis handles to reject background is indicated by *yes/no*.

| Desired signal | main background | up/down | energy | direction | time |
|---|---|---|---|---|---|
| Atm. $\nu$ | Atm. $\mu$ | yes | no | no | no |
| $\nu$ from AGN (diffuse) | Atm. $\nu$ & $\mu$ | yes | yes | no | no |
| UHE $\nu$ (diffuse) | Atm. $\mu$ | no | yes | no | no |
| $\nu$ from point sources | Atm. $\nu$ & $\mu$ | yes | yes | yes | no |
| $\nu$ from GRB | Atm. $\mu$ | yes/no | yes | yes | yes |

The largest signal fluxes are predicted for the integrated diffuse fluxes, e.g. high-energy neutrinos from all active galactic nuclei (AGN). However, the background rejection is quite difficult, since only energy and the up/down criteria can be used to discriminate backgrounds. Tight selections with these variables are required to reduce the background and achieve a sufficiently pure signal sample.
When searching for signals from point sources, the background is lower, because the search bin is smaller. This allows the use of less stringent data selection criteria, which yields a larger effective area. However, the predicted fluxes from a single source are small.
An ideal case is the search for neutrinos coincident with gamma ray bursts (GRB): a direction and a time stamp are provided by satellite data. This allows for high signal efficiencies and thus largest effective volumes.

## 3. The AMANDA Experiment

The present AMANDA-II experiment, shown in figure 4, is a lattice of 677 optical modules (OM), which are deployed in the ice along 19 strings at the geographic south pole. Each optical module is a spherical glass pressure vessel, which contains an 8 inch PMT and its electronics. The OMs are connected to the counting room at the ice surface by power and signal cables. The trigger is generated and the signals are digitized with conventional VME/NIM/CAMAC electronics. The optical modules form a detector of almost cylindrical geometry with 100 m radius at depths between 1500 m and 2000 m beneath the ice surface. This volume corresponds to about 15 Mt of ice. The inner core of AMANDA-II is the AMANDA-B10 detector, which is the inner ten strings with 302 OMs. It was completed in February 1997. The results,

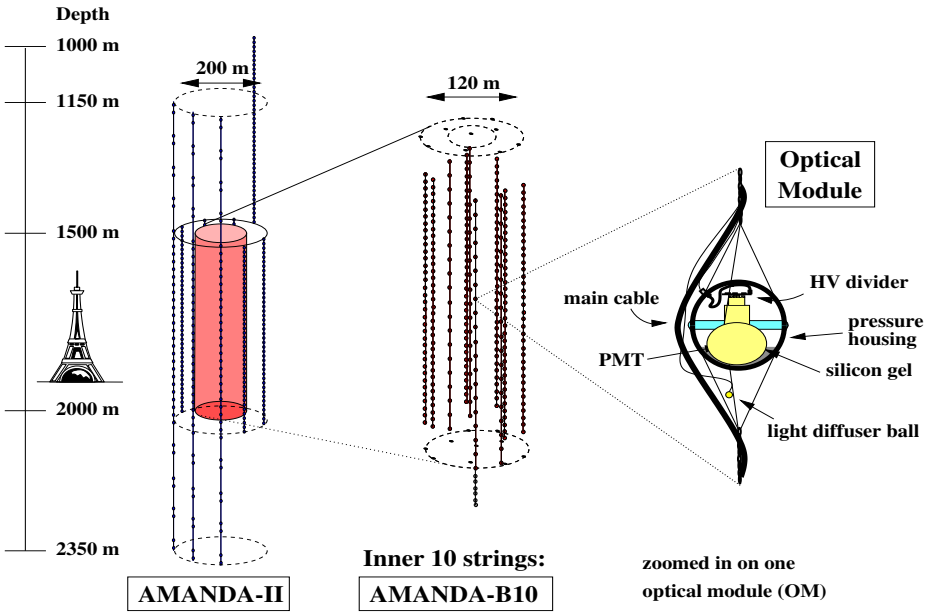


Fig. 4. The AMANDA-II detector complex after its completion in the beginning of 2000.

presented in this paper, were obtained primarily from the first year of operation of this detector.

Unlike other neutrino telescopes, AMANDA continuously measures atmospheric muons coincident with events detected by the surface air shower array: SPASE.[13] These muons are used to survey and calibrate AMANDA.[14] The measurement of the high-energy muon component also improves the cosmic ray composition analysis of the SPASE experiment.[15]

Table 2. Summary of the AMANDA-II construction

| Year | Name | Strings | | OMs | | Main purpose | OM technology |
|---|---|---|---|---|---|---|---|
| | | new | total | new | total | | |
| 1996 | AMANDA-B4 | 4 | 4 | 86 | 86 | Ice properties, Drilling | Coax |
| 1997 | AMANDA-B10 | 6 | 10 | 216 | 302 | Detection of atmospheric $\nu$ | Twisted pair |
| 1998 | AMANDA-B13 | 3 | 13 | 122 | 424 | Depth profile of optical properties | Analog optical |
| 2000 | AMANDA-II | 6 | 19 | 253 | 677 | Search for HE $\nu$ | Analog optical, Digital OM |

The AMANDA collaboration has built four detectors, each encompassing its predecessors, as shown in table 2. One important purpose of these detectors is the development of technologies to construct a km$^3$ size experiment: IceCube at the South Pole. This is illustrated by different geometries of installations and steadily

improved technology in the used OMs. AMANDA-B4 uses a passive OM with single coaxial cable connection for power and signal[16]. AMANDA-B10 improved the signal transmission by using twisted quad cables. AMANDA-B13 uses optical fibers to transmit the analog PMT signal to the surface[17] with almost no distortion. AMANDA-II includes 42 PMTs to test an advanced concept for IceCube. Active electronics digitize and analyze the PMT signal inside the OM and transmit the digital data to the surface [11].

Several *in situ* light sources are used to calibrate the detector and measure the optical properties of the ice. These include pulsed laser and LED modules and optical fibers from the surface terminated with a diffuser. The optical fibers are illuminated with a tunable dye laser or a high-power solid-state laser. The detector hardware, the surface electronics and the calibration procedures are described in more detail in Refs.[16,18].

The optical parameters of the ice depend on wavelength and depth. The absorption length is $\sim 110$ m (at 400 nm, with a strong wavelength dependence) and the effective scattering length is $\sim 25$ m, with a significant depth dependence. The optical properties of the ice are discussed in detail in Ref.[19].

Events are reconstructed with a maximum likelihood method, which models a detailed description of the scattering and absorption of photons in the ice into a probability for the measured arrival times at the PMTs. Fits are performed both for a muon track and a spherical cascade hypothesis. Event reconstruction procedures are largely explained in Ref.[20].

## 4. Results from AMANDA-B10

### 4.1. *Atmospheric neutrinos*

Atmospheric neutrinos are an important signal, because they can be used to understand the detector performance, and particular emphasis was put into their analysis for AMANDA-B10. The huge background of down-going muons exceeds the flux of neutrino induced up-going muons by almost six orders of magnitude. This sets stringent requirements on the quality and robustness of the pattern recognition and the understanding of rare backgrounds.

Precise Monte Carlo simulations were developed to achieve a quantitative understanding of the signal and the rare backgrounds. Several high statistics Monte Carlo productions were performed, each based on improved understanding of the detector. Two working groups performed independent analyses, which differ in methodical aspects and the particular choice of selection parameters.[21]

The analysis is based on $10^9$ events taken with the AMANDA-B10 detector during the austral winter period from April to November 1997. The trigger requires $\geq 16$ OMs reporting a signal within 2.5 $\mu$s at the surface, resulting in an average trigger rate of 75 Hz. The dead-time corrected integrated live-time is about 130 days. A subset of 260 OMs, which were stable over the whole period are used.

Table 3. Results for atmospheric neutrinos

| | Analysis 1 | Analysis 2 | Common | Combined |
|---|---|---|---|---|
| Experiment | 223 | 204 | 102 | 325 |
| atm.$\nu$-MC (A) | 378 | 265 | 119 | 524 |
| atm.$\nu$-MC (B) | 237 | — | — | — |
| Background | 5-10% | 10% | — | — |

After several subsequent levels of selections, both analyses were able to achieve a background rejection ratio of approximately $10^8$. Both yield a sample of $\geq 200$ neutrino induced events, including about 10% background events (see table 3). The combined sample of both analyses contains 325 events. The celestial distribution of these events is shown in figure 7 (left). The absolute number of events is less than expected from the simulations. As discussed below, this deficit is consistent with systematic uncertainties. These uncertainties are reflected by the difference between the two simulations (A) and (B). The number of common events, found in both samples, agrees with the MC prediction. Approximately 90% of the simulated events have muon [neutrino] energies between 50 [65] GeV and 1.8 [3.4] TeV. We estimate the effective area [volume] for muons of 1 TeV in this analysis to be about $3 \times 10^3\,\mathrm{m}^2$ $[8 \times 10^6\,\mathrm{m}^3]$.

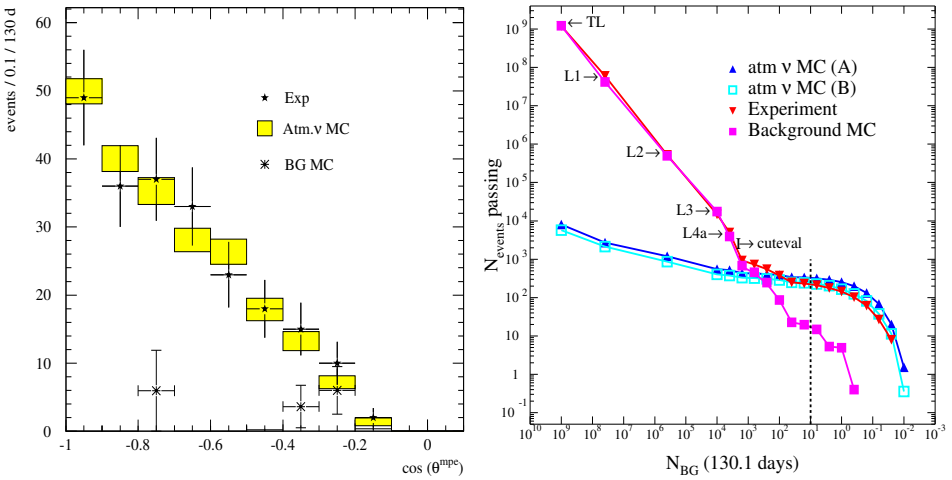


Fig. 5. Results of the AMANDA-B10 atmospheric neutrino analysis. Left: Distribution of reconstructed zenith directions. Right: Number of events as function of the selection (see text).

The characteristics of the selected events are consistent with the expectations for atmospheric neutrinos. For example, the left graph of figure 5 shows the distribution of measured zenith angle compared to the simulation. The detector achieves the largest efficiency for vertical events, which is expected from the cylindrical geometry of the detector.

Figure 5 (right) demonstrates the quantitative understanding of signal and background. It shows the number of events $N_{events}$ as function of the selection. The

selection cuts have been parameterized as function of the estimated number of background events $N_{BG}$, which defines the $x$-axis. The different event samples: atmospheric neutrinos (MC), background from atmospheric muons (MC) and the experimental data are exposed to these selection cuts. The number of events $N_{events}$ which survive the selection are plotted on the $y$-axis. The case of no selection (trigger level TL) corresponds to $\sim 10^9$ events. Gradually enforcing the selection corresponds to smaller numbers of $N_{BG}$ towards the right. Here the experimental number $N_{events}$ follow the numbers from the background MC, since the fraction of signal events is small. At $N_{BG} \approx 500$ the slope of the experimental data changes and the shape follows the expectation from atmospheric neutrinos up to strong selections $N_{BG} \sim 10^{-2}$, where only a few events remain. The final selection corresponds to $N_{BG} = 10$, which is indicated by a dotted line. Two different simulations of atmospheric neutrinos, using different ice parameters, are shown. They reflect the range of systematic uncertainties in the analysis.

Systematic uncertainties are evaluated by a variation of the input parameters to the simulation within their allowed range. We find that the topologies of selected events and their reconstruction accuracy are largely insensitive but that the absolute normalization is affected quite strongly. Here, uncertainties due to the time calibration are small: $< 5\%$. The absolute sensitivity of the OMs contributes with about 15%. The effects of the optical parameters of the ice and its structure are stronger and contribute uncertainties of 20%–40%. The theoretical uncertainties are similar. Most notable is the absolute flux prediction ($\sim 30\%$) and the energy loss during muon propagation ($10 - 20\%$). Compared to these, the effects due to oscillations of atmospheric neutrinos are small: $\leq 5\%$. The observed difference in the predicted event numbers is consistent with these systematic uncertainties.

The number of background events in the final sample is estimated by various techniques: Monte Carlo, experimental distributions, visual inspection of events and the raw detector information. Background arises from physics processes such as muon bundles, bright bremsstrahlung energy losses of the muons and PMT noise. These are found to be well described by the simulation. More difficult are instrumental effects: e.g. cross talk, or the rare backgrounds: e.g. simultaneous muons from independent but coincident air showers. These effects are estimated by a careful inspection of the experimental data for pathological patterns. Different techniques agree well with an estimate of a contamination less than 10% in the final samples.

### 4.2. *Diffuse flux of high-energy neutrinos*

#### 4.2.1. *Muon channel*

The characteristics of the observed neutrino events in the previous section agree with the expectations for atmospheric neutrinos. Therefore, strong contributions from other sources of high-energy neutrinos can be excluded. The low energy events can be suppressed to improve the sensitivity by selections on energy sensitive param-

eters. In particular the number of hit PMTs depends on the energy. High-energy muons produce more light and more PMTs detect a signal.

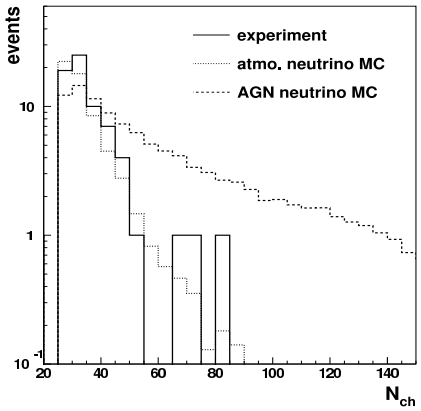


Fig. 6. Distribution of the number of hit PMTs $N_{ch}$ for the selected up-going muon events. In addition simulations for atmospheric neutrinos and AGN neutrinos, assuming a spectrum of $d\Phi/dE = 10^{-5}E^{-2}\mathrm{cm}^{-2}\mathrm{s}^{-1}\mathrm{sr}^{-1}\mathrm{GeV}$, are shown.

Figure 6 shows the number of hit PMTs for a modified selection of neutrinos, which enhances higher energies.[22] The experimental data is consistent with the expectation from atmospheric neutrinos. A strong additional component of high-energy neutrinos would result in an excess of events at higher multiplicities. A selection cut of $N_{ch} > 56$ leads to the observation of three events, consistent with atmospheric neutrinos. The upper limit for a $E^{-2}$ spectrum of extraterrestrial neutrinos is

$$\frac{d\Phi}{dE} < 0.9 \times 10^{-6} E^{-2} \mathrm{cm}^{-2}\mathrm{s}^{-1}\mathrm{sr}^{-1}\mathrm{GeV} \qquad (90\%\ \mathrm{C.L.})\ , \tag{3}$$

within the sensitive region from 10 TeV to 1 PeV. The limit is compared with theoretical predictions in figure 1. We expect a substantial improvement of this limit with the additional data from AMANDA-II,

4.2.2. *Cascade channel*

A similar analysis has been performed to search for cascade-like signals in the AMANDA-B10 data from 1997.[23] The efficiency and accuracy of the reconstruction has been experimentally verified by (a) *in-situ* light sources, which produce a light pattern rather similar to that of cascades and (b) by reconstructing bright catastrophic energy losses, e.g. bremsstrahlung, from down-going muons. These events can be considered as cascade-like. The assumed selection efficiencies can by established experimentally by comparing experimental data with the Monte Carlo simulations.

No event is observed in the energy range 5 TeV–300 TeV. This gives a limit of

$$\frac{d\Phi}{dE} < 6.5 \times 10^{-6} E^{-2} \mathrm{GeV}\mathrm{cm}^{-2}\mathrm{s}^{-1}\mathrm{sr}^{-1} \qquad (90\%\ \mathrm{C.L.}) \tag{4}$$

for the flux of $\nu_e$ and $\bar{\nu}_e$. If one takes the sensitivity to $\nu_\tau$ and the neutral current interactions by all flavors into account, one derives derives a limit of

$$\frac{d\Phi}{dE} < 9.8 \times 10^{-6} E^{-2} \mathrm{GeV cm^{-2} s^{-1} sr^{-1}} \qquad (90\%\ \mathrm{C.L.}) \tag{5}$$

for the sum of all neutrino flavors, assuming flavor ratios of $\nu_e : \nu_\mu : \nu_\tau = 1 : 1 : 1$.

4.2.3. *Extremely high energies*

For energies $> 1\,\mathrm{PeV}$ the Earth becomes opaque to neutrinos. A dedicated analysis attempts to extract neutrino induced single muons with very high-energy from the large flux of down-going atmospheric muons.[24] This is done by an investigation of the event topologies using an artificial neural network. The final selection achieves an effective area of $0.3\,\mathrm{km^2}$ at 1 EeV. The preliminary analysis of 75 days (live-time) from 1997 finds no signal event, which corresponds to a limit of

$$\frac{d\Phi}{dE} < 1.5 \times 10^{-6} E^{-2} \mathrm{cm^{-2} s^{-1} sr^{-1} GeV} \qquad (90\%\ \mathrm{C.L.}) \quad , \tag{6}$$

for the flux of extraterrestrial neutrinos, assuming an $E^{-2}$ spectrum within the region 1.8 PeV–6.3 EeV. The limit is shown in figure 1.

### 4.3. *Point sources*

For the case of point sources, the background is drastically reduced due to the smaller field of view. The optimum sensitivity $\sigma$ for a potential source scales with $\sigma \sim S/\sqrt{B}$, where $S$ is the signal and $B$ the background in each bin. It does not scale with the signal purity $\sim S/B$. The analysis of the search bin size leads to optimum values ranging from 3.5°, which are similar to median angular resolution of AMANDA-B10, up to 6°. It depends on the assumed signal strength and data selection. The selection itself is less rigorous with respect to background when compared with the atmospheric neutrino analysis, which was optimized for signal purity. Point sources are also expected to provide a hard spectrum $\sim E^{-2}$. The selection is optimized for high energies to suppress atmospheric neutrinos.
Two analyses have been performed: The first[25] searches the celestial distribution of the sample of atmospheric neutrinos for anisotropies (see left figure 7). The second approach[26] consequently follows the above considerations and optimizes $\sigma$ and the selection of high energies with good sky coverage, in particular for the horizontal direction. The result is shown in figure 7 right. More events appear due to this weaker selection criteria. About 25% of them correspond to atmospheric neutrinos, and the rest are mis-reconstructed down-going tracks.
Both searches find celestial distribution which are consistent with a random distribution with no significant excess over the background. The second analysis achieves tighter flux limits, except for the case of soft source spectra $\sim E^{-3}$ or sources close to the nadir. Here the analysis based on atmospheric $\nu$ achieves a higher sensitivity. The assumption of an $E^{-2}$ spectrum gives average limits for the up-going

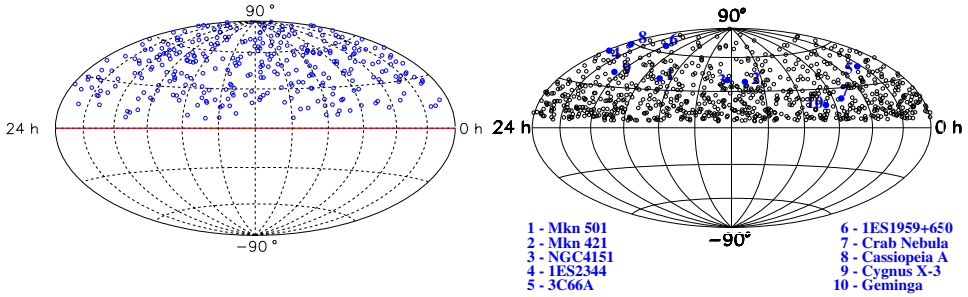


Fig. 7. Celestial distribution of muon arrival directions for the atmospheric neutrino analysis (left) and the dedicated point source analysis (right).

Table 4. Muon and neutrino flux limits on selected sources for $E_\nu > 10\,\mathrm{GeV}$. $N_{obs}$ is the number of observed events in the search bin and $N_{\mathrm{bg}}$ is the expected background. The energy interval, $\Delta E$, contains 90% of the neutrino events. The flux limits are calculated according to a representative survey of models (given in the second column). They are corrected for systematic uncertainty.[26]

| Source | Model | $N_{obs}$ | $N_{\mathrm{bg}}$ | $\Delta E$ TeV | $\Phi_\nu^{\mathrm{limit}}$ $10^{-8}\mathrm{cm}^{-2}\mathrm{s}^{-1}$ | $\Phi_\mu^{\mathrm{limit}}$ $10^{-15}\mathrm{cm}^{-2}\mathrm{s}^{-1}$ |
|---|---|---|---|---|---|---|
| Mkn 501 | $d\Phi_\nu/dE \propto E_\nu^{-1.92}$ | 7 | 3.5 | 1-1000 | 9.5 | 14.6 |
| Mkn 501 | $n_\nu = n_\gamma$ from [27] | 7 | 3.5 | 0.3-20 | 86.0 | 38.9 |
| Mkn 421 | [28] | 4 | 3.7 | 1-1000 | 11.2 | 9.7 |
| NGC4151 | [28] | 5 | 3.6 | 1-1000 | 12.9 | 10.9 |
| NGC4151 | [29] | 5 | 3.6 | 60-2500 | 0.0042 | 5.6 |
| 1ES2344 | $d\Phi_\nu/dE \propto E_\nu^{-2}$ | 5 | 2.9 | 1-400 | 12.5 | 10.3 |
| 3C66A | [28] | 3 | 3.5 | 0.8-250 | 7.2 | 6.6 |
| 1ES1959+650 | $d\Phi_\nu/dE \propto E_\nu^{-2}$ | 4 | 1.7 | 0.8-250 | 13.2 | 9.7 |
| Crab Nebula | $d\Phi_\nu/dE \propto E_\nu^{-2}$ | 2 | 5.6 | 1-1000 | 4.2 | 5.0 |
| Cassiopeia A | $d\Phi_\nu/dE \propto E_\nu^{-2}$ | 3 | 2.2 | 1.8-1000 | 9.8 | 7.6 |
| Cygnus X-3 | $d\Phi_\nu/dE \propto E_\nu^{-2}$ | 2 | 3.4 | 1-1000 | 4.9 | 4.6 |
| Geminga | $d\Phi_\nu/dE \propto E_\nu^{-2}$ | 4 | 7.1 | 1.8-1000 | 6.8 | 9.1 |

muon flux $\Phi_\mu^{90\%}$ from point sources between $4 \cdot 10^{-14} cm^{-2} s^{-1}$ close to the horizon and $0.6 \cdot 10^{-14} cm^{-2} s^{-1}$ for vertical directions. Flux limits for selected candidate sources are given in table 4. These limits for the northern hemisphere were obtained with 130 days of data from 1997. They are comparable to the limits for the southern hemisphere, which were obtained by northern underground detectors with much longer exposure time.[2,30] We expect a substantial improvement with the now available data from the AMANDA-II detector.

### 4.4. *WIMPS annihilation in the Earth core*

The neutralino $\chi$ is a Weakly Interacting Massive Particle (WIMP) and a dark matter candidate proposed by the Minimal Supersymmetric extension of the Standard Model (MSSM). Relic neutralinos can be gravitationally trapped in massive objects, e.g. inside the Earth and concentrate close to the core, where they annihi-

late pair-wise. Neutrinos are produced in the subsequent decays of the annihilation products. Depending on the MSSM parameters one distinguishes soft channels with lower neutrino energies due to annihilation into quark jets (e.g. $\chi + \bar{\chi} \rightarrow b^+b^-$) from hard channels due to decays of gauge bosons and $\tau$ leptons. The experimental signature for annihilation in the Earth is the excess of nearly vertical neutrinos over the background from atmospheric neutrinos, for which the AMANDA experiment has an ideal geometry.

In a dedicated analysis of the data from 1997 no such excess was found, and limits on the muon flux and the neutralino annihilation rate were determined.[31] For hard channels and masses $m_\chi > 500\,\mathrm{GeV}$ the limit on the muon flux is better than $\Phi_{\mu,90\%} \leq 1500\mathrm{km}^{-2}\mathrm{yr}^{-1}$. A similar sensitivity is achieved with the analysis of atmospheric neutrinos, where also no excess of vertical events is found.

The AMANDA-B10 detector with 130 days of exposure has reached a sensitivity, which constrains the theoretically allowed parameter space. It is comparable in sensitivity with other experiments of much longer running time. Analysis of additional data sets from 1998-2002 and improved understanding of systematic uncertainties will provide significantly better limits.

### 4.5. *Relativistic magnetic monopoles*

A magnetic monopole with unit magnetic Dirac charge and a velocity of $\beta = v/c$ close to 1 would emit Cherenkov light along its path, exceeding that of a bare relativistic muon by a factor of 8300. As result one expects spectacularly bright events, with a large fraction of PMTs in the array showing one or several signals. Unlike very high-energy muons, this light is emitted continously, and it is deposited smoothly throughout the detector.

No event with this signature is observed in the data from 1997. The corresponding flux limit is

$$\Phi_{90\%} = 0.62 \times 10^{-16}\mathrm{cm}^{-2}\mathrm{s}^{-1}\mathrm{sr}^{-1} \ , \tag{7}$$

assuming $\beta = 1$. The analysis is restricted to up-going tracks, requiring a minimum monopole mass of $\sim 10^{11}$ in order to remain relativistic after traversing the Earth. The limit is a factor 20 below the Parker bound and a factor 4 better than other limits for $\beta \simeq 1$.

### 4.6. *Gamma ray bursts*

Neutrino events can be searched in coincidence with gamma-ray bursts (GRBs). The direction and burst time are known from satellite observations. The BATSE[32] satellite has detected 304 GRBs in 1997, out of which 78 bursts are from the northern hemisphere and coincident with AMANDA data taking.

The GRB analysis looks for enhancements in up-ward muons over 10 s periods from the bursts direction.[33] For these short time intervals, a relatively soft selection allows for a background rejection of $10^{-3} - 10^{-4}$. This is sufficient for an almost background free analysis for the direction of interest. The selection is optimized for

muon neutrinos in the energy range $10 - 100\,\mathrm{TeV}$. They are simulated according to the predicted energy spectrum of the fire-ball model.[34] This spectrum and thus the number of events strongly depends on an intrinsic model parameter: the boost factor $\gamma$. Taking into account burst to burst fluctuations in energy and distance[35], we expect between 1.1 ($\gamma = 100$), 0.02 ($\gamma = 300$) and $10^{-4}$ ($\gamma = 1000$) events after selection. The achieved effective area is approximately $17000\,\mathrm{m}^2$ for $\gamma = 300$.
The background is estimated for each burst individually by off-time measurements. The background rate is sampled in 10 s time bins $\pm 1\,\mathrm{h}$ around the burst time. It is consistent with the Gaussian expectation.
For the 78 inspected bursts, no burst with a significant excess is found. The derived combined upper limit on the neutrino flux is

$$\Phi_\nu^{90\%} \leq \begin{cases} 10 \cdot 10^{-11}\mathrm{cm}^{-2}\mathrm{s}^{-1} & \text{for} \quad \gamma = 100 \\ 4.8 \cdot 10^{-11}\mathrm{cm}^{-2}\mathrm{s}^{-1} & \text{for} \quad \gamma = 300 \\ 2.1 \cdot 10^{-11}\mathrm{cm}^{-2}\mathrm{s}^{-1} & \text{for} \quad \gamma = 1000 \end{cases} \tag{8}$$

The effective area of AMANDA-II for GRB searches will be approximately $60000\,\mathrm{m}^2$.

### 4.7. *Supernova bursts*

The gravitational collapse of a massive star in our galaxy can produce a detectable neutrino burst in AMANDA. These neutrinos have a mean energy of about 20 MeV. They interact with protons and produce a positron, which propagates about 10 cm through the ice. The light output from individual interactions are far below the detection threshold. Therefore the analysis proceeds in a different way. It takes advantages of the large absorption length and and low noise of the PMTs in the ice: 300-1200 Hz. During a burst multiple neutrino interactions occur within the active volume and lead to a collective noise rate increase of all PMTs. AMANDA records the noise rate of all PMTs in intervals of 0.5 s.
The analysis[36] of the data from 1997 and 1998 (215 days of live time) finds no candidate burst event yielding an upper limit of 4.3 on the rate of stellar collapses in the Milky Way. It has a 70% coverage of our Galaxy at 90% detection efficiency and 1 false trigger per year. A real-time algorithm, which allows AMANDA to join SNEWS[37], a supernova early warning network of neutrino detectors, is in preparation.

## 5. First Results from AMANDA-II

With the completion of the AMANDA-II detector in 2000, the number of PMTs has more than doubled. Simulations predict a more than proportional gain in the detector sensitivity. The reason is, that in addition to the larger volume the larger number of PMTs also allow for an improved pattern recognition. The better background rejection leads to a higher signal efficiency. Also the angular resolution improves from $\sim 3.5^\circ$ in AMANDA-B10 to $\sim 2^\circ$ in AMANDA-II. Initial analysis of the AMANDA-II data experimentally verify this expectation.

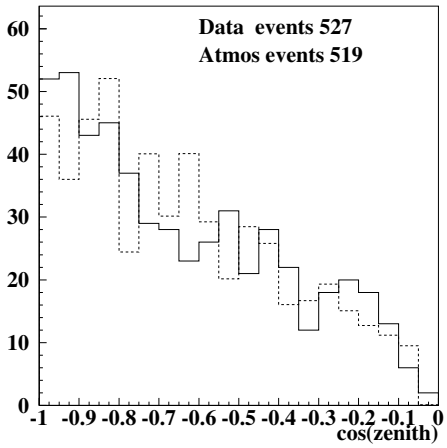


Fig. 8. Zenith distribution of upward-going muons (data, solid line) in the AMANDA-II detector in the year 2000. The expected distribution from atmospheric neutrinos is shown as dashed line.

The preliminary analysis of atmospheric neutrinos demonstrates the increased power of AMANDA-II. In spite of the non-optimized selection cuts and the higher energy threshold, $\sim 100\,\mathrm{GeV}$, of AMANDA-II, more than 500 neutrino induced events have been extracted. This corresponds to a gain of 2.5 in events compared to AMANDA-B10. Figure 8 shows the distribution of zenith angles. Its shape is in agreement with the simulation of atmospheric neutrinos. In comparison to AMANDA-B10 (figure 5) the sensitivity for horizontal events is much better.

The current analyses make use of the better detector performance in order to improve the understanding of systematic uncertainties, which were still relatively large for AMANDA-B10. We expect that the data already acquired in the years 2000-2002 will be sufficient to improve the detector sensitivity by almost one order of magnitude for all physics cases covered by AMANDA-B10.

## 6. Outlook to IceCube

The IceCube detector, consisting of 4800 PMTs deployed on 80 vertical strings around the AMANDA-II detector, is planned to be completed in 2008.

The sensitivity of the conceptual design to various physics cases has been studied with the realistic Monte Carlo simulation and the current analysis chain used for the AMANDA experiment. The effective area is found to exceed $1\,\mathrm{km}^2$ above 10 TeV for the lower hemisphere. In the multi PeV region, where the Earth becomes opaque to neutrinos, the effective area also exceeds $1\,\mathrm{km}^2$ for the upper hemisphere. The angular resolution is approximately 0.7° (median) at energies above 1 TeV and approaches 0.6° near the horizon. The different neutrino flavors can be identified in the energy range 1 PeV–1 EeV.

The estimated performance of the detector is sufficient to probe the model predictions of the studied physics cases.[10] Assuming an $E^{-2}$ spectrum from 100 TeV to 100 PeV, a limit on the diffuse flux of $\nu_\mu$ of

$$\frac{d\Phi}{dE} = 4.2 \times 10^{-9} E^{-2} \mathrm{cm}^{-2}\mathrm{s}^{-1}\mathrm{sr}^{-1}\mathrm{GeV} \qquad (90\%\ \mathrm{C.L.})\ , \tag{9}$$

is obtained after three years of operation. This limit is sufficiently below the W&B bound, (see figure 1). Similar model assumption for point sources lead to a limit of

$$\frac{d\Phi}{dE} = 2.4 \times 10^{-9} E^{-2} \mathrm{cm}^{-2}\mathrm{s}^{-1}\mathrm{GeV} \qquad (90\%\ \mathrm{C.L.})\ , \tag{10}$$

with three years of data. The measurement of 500 GRBs in the lower hemisphere are sufficient to set limits 20% below the calculated flux.[34] For the search for relativistic magnetic monopoles we expect to improve the sensitivity by almost two orders of magnitude, reaching $\Phi_{90\%} \simeq 10^{-18}\mathrm{cm}^{-2}\mathrm{s}^{-1}\mathrm{sr}^{-1}$. The maximum distance to detect a supernova burst is extended clearly beyond the borders of our galaxy.
These studies provide a conservative estimate of the actually achievable performance. More sophisticated data acquisition and analysis techniques, in particular the full wave-form recording of detected signals inside the OMs[11], are expected to significantly improve the detection and reconstruction of neutrino events.

## Acknowledgments

This research was supported by the following agencies: U.S. National Science Foundation, Office of Polar Programs; U.S. National Science Foundation, Physics Division; University of Wisconsin Alumni Research Foundation; U.S. Department of Energy; Swedish Research Council; Swedish Polar Research Secretariat; Knut and Alice Wallenberg Foundation, Sweden; German Ministry for Education and Research; U.S. National Energy Research Scientific Computing Center (supported by the Office of Energy Research of the U.S. Department of Energy); UC-Irvine AENEAS Supercomputer Facility; Deutsche Forschungsgemeinschaft (DFG).

## References

1. G. Domogatsky et al., Nucl.Phys.Proc.Suppl. 110 (2002) 504-506; astro-ph/0112446
2. M. Ambrosio et al., Astrophys.J, 546 (2001) 1038
3. E. Waxman, J. Bahcall, Phys.Rev. D59 (1999) 023002
4. K. Mannheim, R. Protheroe, J. Rachen, Phys.Rev. D63 (2001), 023003
5. J. G. Learned and K. Mannheim, Ann.Rev.Nucl.and Part.Phys. 50 (2000) 679
6. T. K. Gaisser, F. Halzen and T. Stanev, Phys.Rep. 258 (1995) 173
7. C. Spiering, Nucl.Phys.Proc.Suppl. 110 (2002) 443-452
8. R. Wischnewski et al. (The AMANDA Collaboration), Nucl.Phys.Proc.Suppl. 110 (2002) 510-452
9. J. Carr et al., in procedings *Neutrino-2002*, Munich, May 2002, in press
10. The IceCube Collaboration, *Sensitivity of the IceCube Detector to Astrophysical Sources of High Energy Muon Neutrinos*, in preparation for submission to Astropart. Phys.; see also: A. Karle et al. (The IceCube Collaboration), in procedings *Neutrino-2002*, Munich, May 2002, Nucl.Phys.Proc.Suppl., in press

11. A. Goldschmidt (The IceCube Collaboration), procedings 27th ICRC, HE.2.05.01, pp. 1237–1240, Hamburg, Germany, 2001
12. T.K.Gaisser, in procedings *Neutrino-2002*, Munich, May 2002, Nucl.Phys.Proc.Suppl., in press; hep-ph/0209195
13. J. Dickinson et al., Nucl.Instr.and Meth. A 440 (1) (2000) 95
14. X. Bai et al. (The AMANDA and SPASE Collaborations), proceedings 27th ICRC, HE.208, pp. 977–980, Hamburg, Germany, 2001
15. K. Rawlins, PhD thesis, University of Wisconsin at Madison, USA, Oct 2001
16. E. Andres et al. (The AMANDA Colaboration), Astrop. Phys. 13, 1 (2000)
17. A. Karle et al., Nucl.Instr.Meth. A 387 (1997) 274; astro-ph/9611102; DESY-96-186
18. D. Cowen, K. Hanson et al. (The AMANDA Collaboration), proceedings 27th ICRC, HE-237, pp. 1133–1136, Hamburg, Germany, 2001
19. K. Woschnagg, et al. (The AMANDA Collaboration), proceedings 26th ICRC, HE-4.1.15, Salt Lake City, USA, 1999
20. J. Ahrens et al. (The AMANDA Collaboration) *Track reconstruction of Muon Tracks in AMANDA*, in preparation for submission to Nucl. Instr. Meth. A
21. X. Bai et al. (The AMANDA Collaboration) Phys. Rev. D, 66 (1) (2002) 012005
22. G. Hill, M. Leuthold, et al. (The AMANDA Collaboration), Proceedings 27th ICRC, HE.2.03.08, pp. 1113–1116, Hamburg, Germany, 2001, and M. Leuthold, Ph.D. thesis, Humboldt-Universität, Berlin, Germany, Sep. 2001
23. J. Ahrens, et al. (The AMANDA Collaboration), submitted to Phys. Rev. D, astro-ph/0206487
24. S. Hundertmark, et al. (The AMANDA Collaboration), in procedings *Neutrino-2002*, Munich, May 2002, Nucl.Phys.Proc.Suppl., in press, and S. Hundertmark, et al. (The AMANDA Collaboration) Proceedings 27th ICRC, HE.236, pp. 1129–1132, Hamburg, Germany, 2001
25. A. Biron, Ph.D. thesis, Humboldt-Universität, Berlin, Germany, Jan. 2002
26. J. Ahrens, et al. (The AMANDA Collaboration), submitted to Astrophys. J. , astro-ph/0208006
27. Aharonian, F. A., *et al.* 19 99, Astron. Astrophy., 349 11
28. Szabo, A. P. and Protheroe, R. J., V .J. Stenger, J.G. Learned, S. Pakvasa, and X. Tata, ed., 1992, Proc.High Energy Neutrino Astrophysics Workshop(U. Hawaii), World Scientific, Singapore
29. Stecker, F. W., Done, C., Salamon, M. H. and Sommers, P. 1991, Phys.Rev.Lett. 66, 2697, Erratum- ibid. 69 (1992) 2 738
30. S. Matsuno, et al., Proceedings 27th ICRC, HE 2.3, pp. 1065–1068, Hamburg, Germany, 2001
31. J. Ahrens, et al. (The AMANDA Collaboration), Phys. Rev. D 66 (3) (2002) 032006
32. http://gammaray.mcfc.nasa.gov/batse
33. R. Hardtke, G. Barouch, et al. (The AMANDA Coolaboration), Proceedings 27th ICRC, HE.232, pp. 1121–1124, Hamburg, Germany, 2001
34. E. Waxman, J. Bahcall, Phys. Rev. Lett. 78:2292-2295 (1997)
35. J. Alvarez-Muniz, F. Halzen and D. W. Hooper, Phys. Rev. D 62 (2000) 093015 and F. Halzen and D. W. Hooper, Astrophys. J. Lett. 527 L93, 1999
36. J. Ahrens et al. (The AMANDA Collaboration) Astropart. Phys. 4 (2002) 16, 345–359
37. K. Scholberg, astro-ph/9911359